Title

Deciphering the Solvent Effect for the Solvation Structure of Ca2+ in Polar Molecular Liquids

Journal

The Journal of Physical Chemistry B, 124(16)

ISSN

1520-6106

Authors

Ren, Guoxi
Ha, Yang
Liu, Yi-Sheng
et al.

Publication Date

2020-04-23

DOI

10.1021/acs.jpcb.0c02437

Deciphering the Solvent Effect for the Solvation Structure of Ca^{2+} in Polar Molecular Liquids

Guoxi Ren[1,2,3], Yang Ha[4], Yi-Sheng Liu[4], Xuefei Feng[4], Nian Zhang[1,2], Pengfei Yu[1,2], Liang Zhang[6], Wanli Yang[4], Jun Feng[4], Xiaosong Liu[1,2,5,], Jinghua Guo[4,*]*

[1]State Key Laboratory of Functional Materials for Informatics, Shanghai Institute of Microsystem and Information Technology, Chinese Academy of Sciences, Shanghai 200050, China.

[2]CAS Center for Excellence in Superconducting Electronics (CENSE), Chinese Academy of Sciences, Shanghai 200050, China

[3]University of Chinese Academy of Sciences, Beijing 100049, China.

[4]Advanced Light Source, Lawrence Berkeley National Laboratory, Berkeley, CA 94720, USA.

[5]School of Physical Science and Technology, Shanghai Tech University, Shanghai 201210, China.

[6]Institute of Functional Nano & Soft Materials (FUNSOM), Jiangsu Key Laboratory for Carbon-Based Functional Materials & Devices, Soochow University, 199 Ren'ai Road, Suzhou 215123, Jiangsu, China.

*Corresponding author E-mail address: xliu3@mail.sim.ac.cn, jguo@lbl.gov

ABSTRACT

Although the crystal structures for many inorganic compounds are readily available, researchers are still working hard to understand the relations between the structures and chemical properties in solutions, because that is where most of the chemical reactions take place. A huge amount of effort has been put on modeling the ion solvation structure, from the perspectives of both experiments and theories. In this study, the solvation structures of Ca^{2+} ion in aqueous and alcohol solutions at different concentrations were carefully evaluated by Ca K-edge X-ray Absorption Near-Edge Structure (XANES) and Extended X-ray Absorption Fine Structure (EXAFS). Density functional theory (DFT) calculations were also performed to correlate with the experimental data, and then further extended to other similar systems. It was found that the number of coordination solvent molecules decreases with increasing Ca^{2+} concentration and increasing solvent molecule sizes. From the EXAFS data, the first solvation shell of Ca^{2+} split into two Ca-O distances in methanol solution and the counter ion Cl^- might also be within the first shell at high concentrations. For the first time, the effects of solvent with different polarities and sizes on the ion solvation environment were systematically evaluated.

Keywords: Ca^{2+} ion, solvation structure, concentration dependence, alcohol solution, EXAFS, DFT

1. INTRODUCTION

Ionic solvation is one of the most fundamental but interesting subjects to chemists, especially to those who are interested in reactions in solutions. Many elements have been investigated for ionic solvation, e.g. Na^{+} [1], Mg^{2+} [2], Cu^{2+} [3], Zn^{2+} [4]. Calcium, as an abundant element on earth, plays an important role in numerous biological, chemical and environmental processes. For example, calcium chloride can significantly promote the enzyme activities in blood and control the GABA-transaminase shunt regulation[5], while calcium oxide is an effective catalyst in the production of biodiesel by transesterification of triglycerides with methanol[6]. Besides, calcium ions have been identified as a promising candidate for transporting multiple electrons in secondary batteries because of the high theoretical volumetric capacity of calcium metal anode[7]. Considering the significant importance in the various liquid phase, the solvation structure of Ca^{2+} has been a subject for various experimental and theoretical studies[8-19]. An in-depth understanding of the solvation structure of Ca^{2+} is crucial to explain many chemical processes occurred in solutions, such as the dynamics and kinetics of ion migration influenced by solvation structure[20].

However, it is still not clear about the accurate solvation structure of Ca^{2+} because of the high disorder of Ca^{2+} ion in solution, the labile of the solvent molecules surrounding Ca^{2+}, and the low atomic number of the atoms involved[21]. For example, it is still a controversial issue that whether there exists concentration dependence on the solvation structure of the first shell in water or other polar molecular liquids. Hewish *et al.* used neutron diffraction to find that the coordination number and configuration of Ca^{2+} are strongly dependent on the concentration of hydration structure[8]. Meanwhile, from the theoretical point of view, Chialvo *et al.* thought that calcium hydration number decreases incessantly from 8 to 3.9 with concentration varying from dilute to saturation[9]. a recent study combined X-ray diffraction and ab Initio study found that the coordination number decreases with an increase in concentration[10]. On the other hand, both Badyal et al employed neutron diffraction approach[11] and Albright used X-ray diffraction studies[13] suggested that the hydration of Ca^{2+} is independent of concentration. Although diffraction methods are very popular in solving solvation structures, it focuses on obtaining the long-range

order structure for all ion-water, ion-ion, and water-water interactions. And few studies focus on whether concentration dependence exists in other polar molecular liquids. Therefore we also need a systematic study on the local structure and different solvents to solve this problem. Moreover, there is still not a clear picture about the solvation structure of Ca^{2+} in alcohol solutions. Only a few solvation studies can be found in methanol. For instance, Dang *et al.* suggested that there are about 6 methanol molecules around the Ca^{2+} in diluted methanolic solution by molecular dynamics[14]. Kosztola´nyi *et al.* also used molecular dynamics to speculate that the Ca^{2+} ions are surrounded by 8 methanol molecules for the diluted solution, 7.7 for the 1 mol L^{-1} solution, and extensive Ca-Cl contact ion-pairs in 2 mol L^{-1} methanol solution[15]. While Megyes et al. combined diffraction (X-ray and neutron) study and molecular dynamics simulation to find that in 1 mol L^{-1} solutions, the Ca^{2+} ion is surrounded by six methanol molecules and in 2 mol L^{-1} solution, contact ion-pairs can also be found[10, 16]. Through these literatures, we feel there needs a systematic study on solvation structure in different solvents to bring up the big picture of this field.

X-ray absorption spectroscopy (XAS) is one of the most powerful tools that provides insight into the electronic structure of selected absorbing atoms. In particular, XAS can give detailed electronic information on the unoccupied states right near the Fermi level, such as ligand structure and coordination number, which are strongly affected by the solvation structure around the absorption atoms. Calcium can be studied by soft X-ray absorption at Ca L-edge XAS[22-25] and hard X-ray at Ca K-edge XAS[12, 26-27]. The Ca L-edge XAS corresponds to the transition from Ca 2p electron to the unoccupied Ca 3d empty orbitals, which mainly focuses on the absorbing atom. While the Ca K-edge XAS relates to the transition from Ca 1s electron to the unoccupied Ca 4p states, whose spectra called X-ray Absorption Fine Structure (XAFS). The XAFS is divided into a low-energy region (-20–50 eV) called X-ray absorption near-edge structure (XANES), and a high-energy region (50–1000 eV) termed extended X-ray absorption fine structure (EXAFS). For relatively large disordered systems, the XAFS spectra can determine the statistical properties of the distribution of atoms relative to the central absorbers, which provide the information of the precise local structures. This process is highly dependent upon the symmetry of the local atom

shell and hence provides an independent measure of the local hydration symmetry. Moreover, unlike diffraction methods providing the long-range order structure for all interactions, XAFS probes the local environment about a specific ion of interest without interfering signals from other atoms in the system. This makes XAFS one of the most accurate structure analysis methods for the first-shell region about the ion. Therefore, XAFS has been widely applied to investigate the solvation structure[3-4, 28-30]. In addition to XAS technology, quantum chemistry calculations are also frequently used in modern chemistry research to provide additional insights into experimental results[31-32]. After collecting a large amount of XAFS spectra, Density function theory (DFT) calculations are employed to calculate both the geometric structures and electronic structures of the metal site. The calculated geometric structures are correlated with the EXAFS results, while calculated electronic structures simulated spectra are correlated with the XANES region and help to assign the peaks[33-34].

In this work, we systematically investigate and compare the solvation structure of Ca^{2+} in various polar molecular solvents, including water, methanol, and ethanol, using in-situ, ex-situ XAFS combined with the DFT calculations. We aim to prove the concentration dependence of the first shell structure in different solutions, explain the effect of different polar molecules solvents on the solvation structure. More importantly, we put forward the more fine first shell solvation structure picture of Ca^{2+} in water and methanol, rather than only a coordination number. Moreover, we explore the solvation environment for some other metal ions in aqueous solutions by DFT to further extend our study to a more general level. Our present study sheds light on the picture of the solvation shell of Ca^{2+} and helps to guide the development of XAFS and DFT in studying other ionic solvation.

2. METHODS

2.1 Sample preparation

Part of the analysis involved studies of well-characterized reference samples including $CaCl_2$, $CaCl_2{\cdot}2H_2O$, and $CaCl_2{\cdot}6H_2O$. The anhydrous calcium chloride salt (≥ 99.99% purity)

was obtained in the ultra-dry powder form from Sigma Aldrich. The dihydrate (≥ 99.0% purity) and the hexahydrate (≥ 99.0% purity) were bought in the particle and slice form respectively from Sigma Aldrich too. Dissolving different concentrations $CaCl_2$ in Methanol and ethanol was prepared using 99.99% $CaCl_2$ (Aldrich Chemicals, Lot #499609), 99.9% Methanol (Aldrich Chemicals, Lot # 1060020500) and 99.9% ethanol (Aldrich Chemicals, Lot # 1009800500). All glassware was pre-washed using methanol and ethanol followed by several rinses using the same solution. Four concentration solutions were prepared: 0.5 mol/L, 1.0 mol/L, 1.5 mol/L and 3.0 mol/L. It was worth noting that the saturated concentration of $CaCl_2$ in methanol and ethanol solution was 2.1 mol/L and 1.8 mol/L respectively, so the 3.0 mol/L solution was considered a supersaturated solution. Because both the pure salt and the solution were hydrophilic, storing and handling of these compounds took place in a dry N_2 glove box. Finally, the liquid solution XAFS samples were contained within a 70 um Ca-free plastic heat sealed pouch, which was preventing exposure to air when testing. Besides, 18 MΩ doubly deionized water was used for dissolving different concentrations $CaCl_2$ in H_2O, and it stored in sealed pouches as well. The concentration configuration of $CaCl_2$ in H_2O was 0.5, 1.0, 1.5, 3.0, 5.0 mol/L and 10.0 mol/L, which labeled 0.5 M, 1.0 M, 1.5 M, 3.0 M, 5.0 M, and 10.0 M. The 10.0 mol/L was an over-saturated solution too, because the saturated concentration of $CaCl_2$ in H_2O was 6.7 mol/L. All the sample preparation was done at room temperature.

2.2 XAS Experiments

The Ca L-edge XAS spectra were measured at beamlines 7.3.1 and 8.0.1 at the Advanced Light Source (ALS), Lawrence Berkeley National Laboratory with the storage ring condition of 1.9 GeV and 500 mA current in multi-bunch operation mode. The in-situ Ca K-edge XAFS spectra were measured at beamlines 5.3.1 and 10.3.2. Beamline 5.3.1 uses Si (111) monochromator, operating at 2.1 KeV to 12.5 KeV with beam size 100 um * 100 um with an energy resolution of 0.8 eV at 2.5 KeV, and Beamline 10.3.2 used Si (111) monochromator, energy ranging from 2.1 to 17 KeV with a tunable spot size ranging from 0.8 * 0.8 μm^2 up to 8 *

5 μm^2 and resolving power (E/ΔE) 7000 at 10 KeV. The liquid samples measured at room temperature were positioned at a normal incidence of the x-ray beam. The K-edge fluorescence XAFS spectra were collected using a silicon drift fluorescence detector placed at 45° to the X-ray beam. Baseline I0 was measured using an in-line nitrogen-filled ionization chamber situated in front of the sample. The XAFS spectra were calibrated using $CaCl_2$ spectra by setting the position of the white line to 4042.6 eV. The raw spectra were processed and normalization applied the Athena software[35] and XANES spectra presented here were all the smooth used the 3 points adjacent averaging method. For EXAFS spectra, about 7 scans were averaged to get the high-quality signals in K space. EXAFS spectra were fit using the Feff6 code within the program suite Artemis[35]. The Ca χ(k) data were weighted by k^2 using a Hanning window between $2.8< k < 10.5$ $Å^{-1}$ and the χ(R) fitting in the region of $1< R < 3.5$ Å.

2.3 DFT calculations

DFT calculations were introduced to bring more insights into our data analysis, both for the geometric structures and the electronic structures. We mainly used DFT calculations to model the Ca^{2+} environment and assisted peak assignment in XANES. Geometry optimization was performed using Gaussian 09 package[36], with hybrid functional B3LYP and 6-311+G(d) basis set, in the corresponding solvent (water or methanol) using the Polarizable Continuum Model (PCM). Time-dependent DFT (TD-DFT) calculations were performed using ORCA package[37-42] to calculate all the transitions from Ca 1s to the valence states and simulate the Ca K-edge XANES results, using the crystal structure of the solid or the optimized structures from the previous step, with CAM-B3LYP functional, def2-TZVPP basis set and zeroth-order regular approximation (ZORA) approach. The TD-DFT results were plotted out using Voigt peak shape, with 0.5 Gaussian widths and 0.5 Lorentzian widths using Avogadro (ORCA enhanced version). All calculated transitions were shifted 42 eV systematically to match with the experimental results. The TD-DFT simulated Ca K-edge XAS is shown in figure S2. Both the relative peak energies and the intensities are in good agreement with the experimental results. Then the Mulliken

population analysis (Table S1) of acceptor orbitals in major transitions were used to help peak assignment in spectroscopic analysis.

3. RESULTS

3.1 XANES analysis of reference compounds

We first measured the Ca K-edge XANES spectra of the three reference samples ($CaCl_2$, $CaCl_2{\cdot}2H_2O$, $CaCl_2{\cdot}6H_2O$), as shown in Figure 1a.

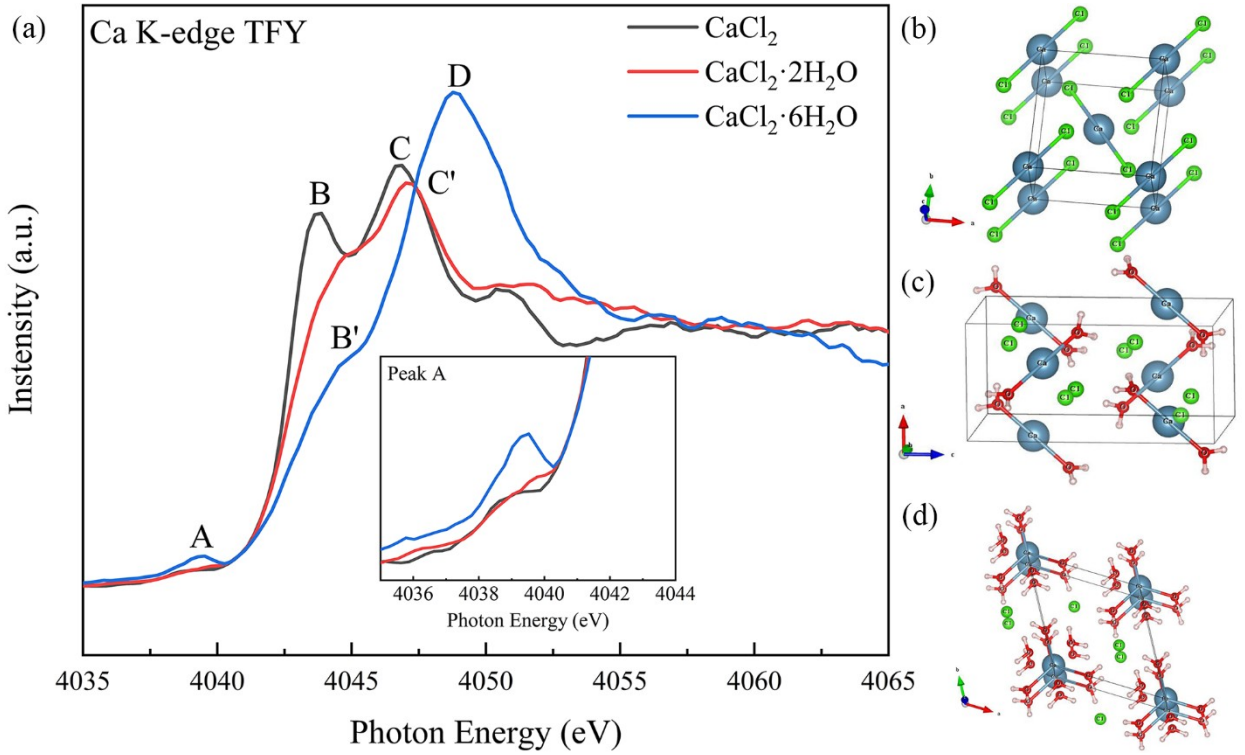

Figure1. (a) Ca K-edge XANES of $CaCl_2$, $CaCl_2{\cdot}2H_2O$, $CaCl_2{\cdot}6H_2O$ with its pre-edge (as an inset) of XANES. (b) crystal structure of $CaCl_2$. (c) crystal structure of $CaCl_2{\cdot}2H_2O$. (d) crystal structure of $CaCl_2{\cdot}6H_2O$

3.1.1 Crystal structure of three solid samples

The crystal structure of $CaCl_2$[43] is the orthorhombic Pnnm space group (Figure 1b). Six Cl atoms are surrounding Ca, in which two of them in the axial position at 2.70 Å and the other four are in the equatorial plane at 2.76 Å. In $CaCl_2{\cdot}2H_2O$[44] (Figure 1c), the space group changes to

Pbcn. Two axial sites are changed to the oxygen from water molecules at a distance of 2.31 Å, and four Cl atoms in the equatorial plane at 2.74 Å. The crystal structure of $CaCl_2 \cdot 6H_2O$[45] is in the trigonal P321 space group. The center Ca is surrounded by nine water molecules without any Cl in the first coordination shell (Figure 1d). The six oxygen atoms at a distance of 2.59 Å form a triangular prism with Ca at the center, while the other three oxygen atoms project out from the vertical faces at a shorter distance of 2.45 Å.

3.1.2 Peak assignment

Next, we compare the Ca K-edge XANES of three samples. the three main features in each spectrum are marked as A, B, and C for $CaCl_2$, A, B', and C' for $CaCl_2 \cdot 2H_2O$, and A, B', and D for $CaCl_2 \cdot 6H_2O$, respectively.

The pre-edge feature A (inset of Figure 1a) is an important probe of the coordination environment at the absorbing center[46-47]. This small feature is attributed to the transition from Ca 1s electron to the unoccupied Ca 3d hybrid states. In the case of $CaCl_2$ and $CaCl_2 \cdot 2H_2O$, the first coordination shell structure is a pseudo octahedron with a shorter distance on-axis direction. The 1s-3d dipole transition is formally forbidden for octahedral symmetries. But for the six coordination pseudo-octahedral compounds, there are low-intensity dipole allowed 1s to (3d+np) transitions because the compression of the Ca−O axial bond reduces symmetry and increases the p−d mixing hybrid states. Nevertheless, for the sample of $CaCl_2 \cdot 6H_2O$ with 9 coordination water, the intensity is significantly enhanced because the central symmetry is broken and more p states mix in the d orbitals. The specific peak of three reference samples is fitted by Voigts function and displayed in Table S2. Furthermore, owing to the Ca L-edge XAS also related to transitions to unoccupied 3d states, we compare the Ca L-edge XAS spectra of three reference samples. As shown in Figure S1, the intensity of peak a1 relative to peak a2 and peak b1 relative to peak b2 indicates the magnitude of the crystal field. This suggests that $CaCl_2 \cdot 6H_2O$ has a different crystal field parameter from $CaCl_2$ and $CaCl_2 \cdot 2H_2O$. The spectra of $CaCl_2$ and $CaCl_2 \cdot 2H_2O$ are very similar, suggesting that they have a similar Ca site structure. The analysis of Ca L-edge XAS corresponds well to the crystal structure, which verifies the correlation between the pre-edge of

Ca K-edge XANES and crystal structure. Therefore, we can estimate the change of the local structure around the Ca^{2+} through the evolution of the pre-edge feature.

Peak B and C are all attributed to the 1s to 4p transition. peak B corresponds to the transition to the 4p state of the Ca^{2+} ion, while the second prominent peak C relates to the transition to the p-like states arising from the 4p hybrid state between Ca and Cl. The previous study confirms this assignment via Cl K-edge XAS of $CaCl_2$[48]. This assignment is also confirmed by the TD-DFT calculated transitions shown in Figure S2. Based on the Mulliken population analysis, the contribution of the peak B is mainly from the p orbitals of Ca, However, There is more contribution from the s and p orbitals of Cl in peak C than in peak B.

Peak D is related to the transition from Ca 1s to Ca-O hybrid orbitals, which is supported by XAFS of CaO[49] and other study[12]. There are 33% p characters from Ca and 58.5% s and p characters from O in peak D shown in TD-DFT calculated transitions, which verifies the transition to Ca-O hybrid orbitals.

Peak B' also arises from the transition of 1s to 4p state of Ca. It can be seen that as H_2O replaces Cl^- near the Ca^{2+}, the ionic bond becomes the coordination bond, which leads to the lone pair electrons on the oxygen of H_2O donating to the Ca^{2+} unoccupied state through hybridization. The charge transfer increases the energy gap between the 1s and 4p unoccupied states and reduces the number of transitions that can be made. Therefore, compared to peak B, peak B' not only moves to high energy but also decreases in intensity. And with increasing the number of coordination oxygen atom, the energy position of Peak B' gradually shifts to higher energy accompanied by the intensity decreasing. The TD-DFT calculated transitions also show some p orbitals from O contributing to this transition.

3.2 XANES analysis of the solution samples

The Ca K-edge XANES spectra of $CaCl_2$ were in different solvations with different concentrations were then measured to be systematically compared.

3.2.1 $CaCl_2$ in aqueous solution

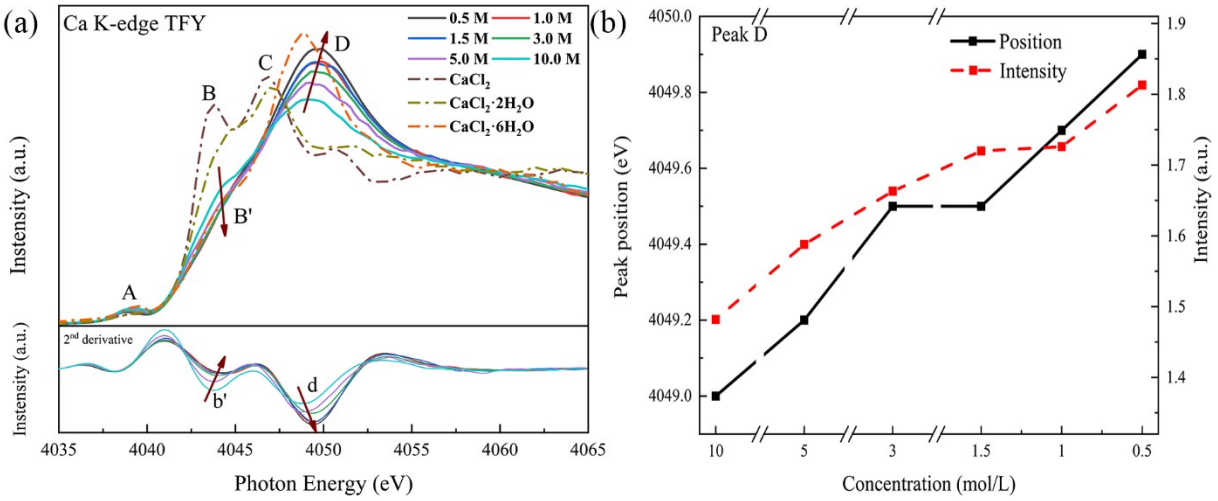

Figure2. (a) Absorption spectra and the corresponding second derivatives of the Ca K-edge for different concentration $CaCl_2$ in water. The dotted line is the XANES of Ca K-edge for solid samples. (b) energy shift and intensity evolution of peak D at the Ca K-edge with different concentrations.

In Figure 2a, the Ca K-edge XANES spectra at different $CaCl_2$ concentrations in water are compared. Like the solid sample, there are three major features labeled as A, B' and D. The peak B' and peak D are changing with concentration and can be further confirmed on the second derivatives

Firstly, we focus on the peak B'. with the concentration decreasing, peak B' moves to high energy and decreases in the intensity. According to the analysis of peak B' in solid samples, the number of coordination oxygen is growing with concentration changing. It is because that the electron charge transfer from the coordination O becomes stronger and the unoccupied states of Ca^{2+} 4p states become less.

Secondly, we talk about peak D. Figure 2b showing the evolution of peak D reveals that with the concentration reducing, the energy position shifts to higher energy and the intensity increases. We first focus on the evolution of energy position. By comparing XANES spectra of $CaCl_2{\cdot}2H_2O$ and $CaCl_2{\cdot}6H_2O$ and combining the meaning of this peak, we can know that the energy of peak D is strongly influenced by the amount of water and the enhanced role of H_2O. A previous study also supports this view. Sowery *et al*. took a systematic study of a range of

calcium/oxygen containing compounds showing that there is a linear correlation between the number of coordination oxygen atoms and edge position, and the edge energy position of peak Ca-O shifts to higher with the number of coordination O increasing[50]. We thus can approximately estimate the number of coordination O around Ca^{2+} by the energy position of peak D. Then we focus on the change in intensity of Peak D. The peak D corresponds to the transition to the Ca-O hybrid orbitals. Its growth in intensity with concentration reduction indicates that the number of transitions to empty hybrid orbitals of O is increasing and the number of coordination O around the Ca^{2+} is growing gradually. Through the analysis of peak D, we can also prove the number of coordination oxygen is growing with concentration decreasing. Furthermore, interestingly, the peak D of XANES for 10.0 M solution has a similar energy position of that for $CaCl_2{\cdot}6H_2O$.Thus, we think there is the similar number of coordination O around Ca^{2+} between 10.0 M and $CaCl_2{\cdot}6H_2O$. But we also need to pay attention to the fact that the intensity of peak D of XANES for 10.0 M is much lower than that for $CaCl_2{\cdot}6H_2O$. A possible explanation is that the Ca-O interreaction in the liquid is weaker than in solid. Because the Ca-O bond distance is longer in water solution, and the H_2O molecules around Ca^{2+} are dynamic equilibrium in solution resulting in the bond between Ca^{2+} and H_2O changing frequently. Therefore the transitions to the hybrid orbitals of Ca-O decrease, the intensity of peak D decreases and the full width at half maxima (FWHM) of peak D becomes larger. Our explanation is further verified by comparing the XANES between the solid $CaCl_2{\cdot}6H_2O$ and liquid $CaCl_2{\cdot}6H_2O$ (after melt). As shown in Figure S3, the intensity of peak D for liquid $CaCl_2{\cdot}6H_2O$ is lower than that for solid $CaCl_2{\cdot}6H_2O$. And the XANES spectra are almost the same for liquid $CaCl_2{\cdot}6H_2O$ and 10.0 M.

Finally, peak A needs to be concerned. An expanded view of peak A is shown in Figure S4.1. Further assessment is made by fitting the peak A using the Voigts function with subtracting the baseline. The detailed fitting curve is shown in Figure S4.2. Table S2 presents the summary statistics for peak position and pre-edge intensity. The energy of pre-edge peak A remains conserved, while the changing in intensity indicates change in symmentry at different concentrations.

Through the analysis of peak B', peak D and peak A, we think that the hydration structures are dependent on the concentration.

3.2.2 $CaCl_2$ in the alcohol solution

We also measured the Ca K-edge XANES spectra of different concentrations $CaCl_2$ in methanol and ethanol shown in Figure S5.1 and Figure S5.2 respectively. Like water, the evolutions of peak D in XANES of methanol and ethanol are shown in Figure S5.3. We can observe the same trend for peak A, peak B' and peak D in XANES in methanol and ethanol solution. Therefore, the number of coordination oxygen is also dependent on the concentration in methanol and ethanol solutions. Combined with the analysis of the XANES of different concentrations $CaCl_2$ in different solutions, we can reasonably believe that there exists a concentration dependence on the solvation structure.

3.2.3 Solvents effect

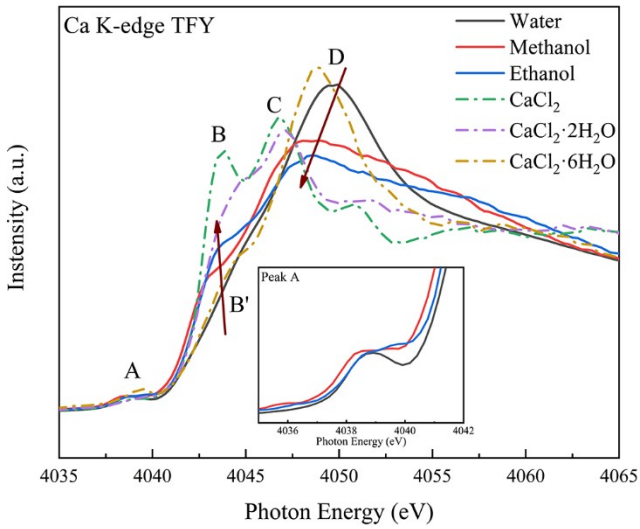

Figure3. XANES spectra of Ca K-edge for 0.5mol/L $CaCl_2$ in water, methanol, and ethanol with(as an inset) its pre-edge of XANES. The dotted line is the XANES of Ca K-edge for solid samples.

Figure 3 displays the XANES spectra of Ca K-edge for 0.5 mol/L $CaCl_2$ in water, methanol, and ethanol. The XANES spectra of Ca K-edge for 1.0 mol/L,1.5 mol/L, and 3.0 mol/L $CaCl_2$ in water, methanol, and ethanol are shown in the Figure S6.1, S6.2, and S6.3 respectively. We can

find that, as the solvent changes from water to methanol and then to ethanol, the peak B' moves to lower energy and higher intensity and the peak D moves to lower energy and lower intensity. According to the analysis above, we can explicitly tell that at the same concentration, Ca^{2+} has less coordination O in ethanol than in methanol and less coordination O in methanol than in water. It is worth noting that the peak D of XANES for 0.5 mol/L $CaCl_2$ in methanol and that for $CaCl_2 \cdot 6H_2O$ have the same energy position, which is similar to the peak D of XANES for 10.0mol/L $CaCl_2$ in water. Moreover, the peak D of XANES for 0.5 mol/L $CaCl_2$ in ethanol even has a lower energy position than it in methanol. Therefore, We can conclude that the number of coordination O around Ca^{2+} for 0.5 mol/L $CaCl_2$ in methanol is not only similar to the number of coordination O around Ca^{2+} for $CaCl_2 \cdot 6H_2O$ and 10.0 mol/L $CaCl_2$ in water, but also more than the number of coordination O around Ca^{2+} for 0.5 mol/L $CaCl_2$ in ethanol. The peak A, as shown in the inset, is very sensitive to the local structure and has some divergences in different solutions, illustrating their ligand field are different.

3.3 EXAFS analysis of the solution samples

To further understand how the solvation structure changes, we fit EXAFS to obtain the coordination number and bond distance around the Ca^{2+}.

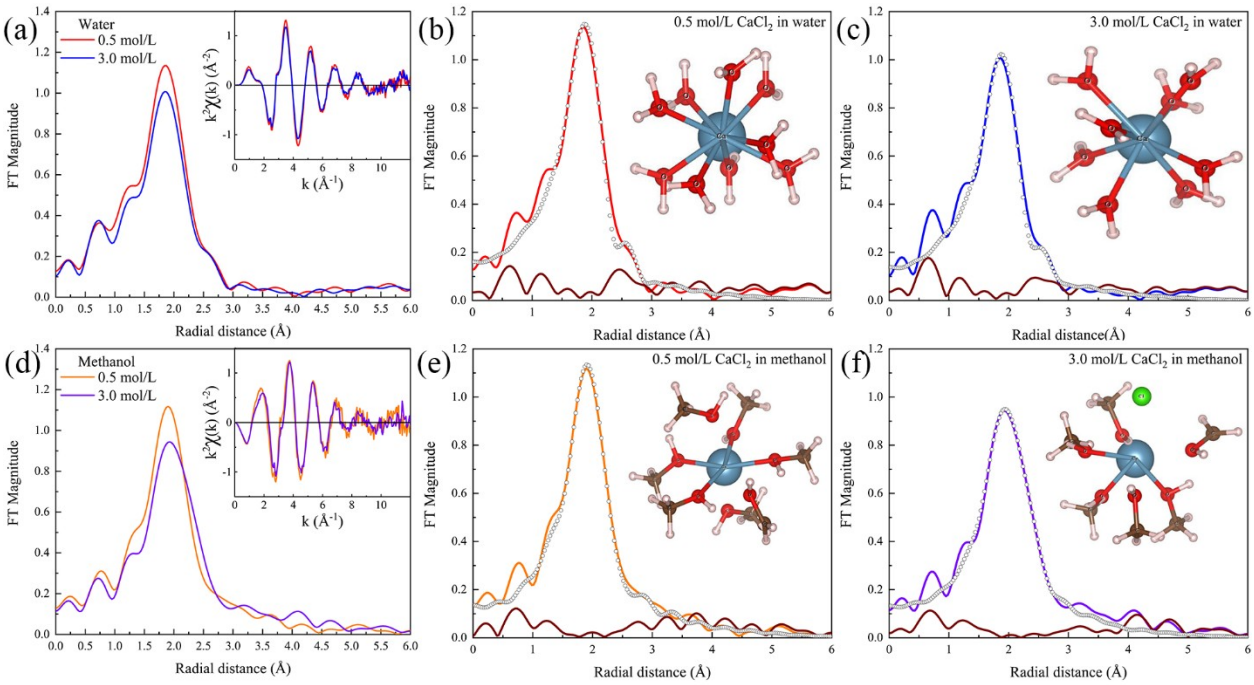

Figure4. (a) The Fourier transform spectrum of the EXAFS for 0.5 mol/L(0.5 M) and 3.0 mol/L(3.0 M) $CaCl_2$ in water with their EXAFS spectrum (as an inset). (b) The Fourier transform spectrum of the EXAFS (red solid line) and fit (open cycle) for 0.5 mol/L $CaCl_2$ in water with its structure(as an inset). Brown solid line is the unfit residual. (c) The Fourier transform spectrum of the EXAFS (blue solid line) and fit (open cycle) for 3.0 mol/L $CaCl_2$ in water with its structure(as an inset). Brown solid line is the unfit residual. (d) The Fourier transform spectrum of the EXAFS for 0.5 mol/L and 3.0 mol/L $CaCl_2$ in methanol with their EXAFS spectrum(as an inset). (e) The Fourier transform spectrum of the EXAFS (yellow solid line) and fit (open cycle) for 0.5 mol/L $CaCl_2$ in methanol with its structure (as an inset) and only the nearest neighbor O is bonded. Brown solid line is the unfit residual. (f) The Fourier transform spectrum of the EXAFS (purple solid line) and fit (open cycle) for 3.0 mol/L $CaCl_2$ in methanol with its structure (as an inset) and only the nearest neighbor O is bonded. Brown solid line is the unfit residual.

3.3.1 Aqueous solution

The contributions from nearest neighbor atoms around Ca^{2+} are qualitatively resolved in the χ(R) results presented in Figure 4a. The χ(R) functions are generated by Fourier transformation of χ(k) data and represent the partial pair distribution functions convoluted with the photoelectron scattering functions. The inset in Figure 4a shows the k^2 weighted χ(k) data for different $CaCl_2$ concentration in water. The χ(k) EXAFS spectrum attenuates rapidly with a little intensity beyond k = 9 $Å^{-1}$. This behavior was a characteristic feature of the EXAFS of the

solution, which results from the great increase of disorder in the solution system. According to the EXAFS function, the amplitude is associated with the coordination number, and the frequency is related to the bond distance. By comparing the $\chi(k)$ data of 0.5 M and 3.0 M, we can find a little divergence in amplitude, but the frequency is almost the same. Hence there are different coordination numbers between the two concentrations but with a similar bond distance. After we tried various structures, the full fitting for 0.5 M uses a single shell of nine oxygen atoms scatters. However, the best fitting for 3.0 M is a single shell of eight oxygen atoms scatters. The best single-shell fitting for two aqueous solutions are presented in Figure 4b and Figure 4c, respectively, with the final picture of solvation structures shown in their insets. The detailed fitting parameter can be seen in Table S3. The EXAFS fitting implies that, for the 0.5M solvation sphere, the best estimate of coordination number is 9.04 ± 1.40 water molecules and Ca-O distance is 2.39 Å. While for the 3.0 M solvation sphere, the best estimate of coordination number is 8.08 ± 1.11 water molecules and Ca-O distance is 2.40 Å. The high error bar is mainly due to the higher degree of disorder in the solution, which also appears in another EXAFS study[12]. And the large σ^2 value in the fitting implying radial disorder among the Ca–O distances also potentially increases the error bar of the coordination number. But we still roughly know that the coordination number decreases as the concentration increases.

According to our above deduction from XANES spectra, the coordination number for 10.0 M will be less than 0.5 M. But 10.0 M has the same amount of coordination H_2O as $CaCl_2{\cdot}6H_2O$, which also has 9 coordination H_2O structure. To check if this result is contradictory to previous inferences, we look closely at the crystal structure of $CaCl_2{\cdot}6H_2O$. There are two different bond lengths in the first shell for the 9-coordinated water in $CaCl_2{\cdot}6H_2O$, three of which are shorter and the others are longer. Therefore, we can reasonably speculate that the structures between 10.0 M and $CaCl_2{\cdot}6H_2O$ are similar. The water molecules around Ca^{2+} are divided into two different distances in 10.0 M as well, and only three water molecules are the nearest neighbors. To verify this view, we compare the EXAFS results between 10.0 M and liquid $CaCl_2{\cdot}6H_2O$ (after melt). As shown in Figure S7.1, the EXAFS spectra of 10.0 M and liquid $CaCl_2{\cdot}6H_2O$ are

almost the same for both the K space and R space. The best fitting for 10.0 M (Figure S7.2) is a two distance H_2O structure with only 2.44 nearest H_2O and 2.71 farther H_2O. Therefore, the whole process is as follows. The water molecules in the nearest single shell start gradually decrease from 9 with the concentration increasing. And when the nearest water molecules reduce to a certain extent, the water molecules from the outer shell layer will migrate to the inside, where a little further away from the nearest shell. Finally, the water molecules also form a new 9 coordination H_2O structure in the first shell, but it is divided into two distances. However, only the nearest water molecules of the first shell provide the electron charge transfer, affect the peak D and interact with Ca^{2+}.

3.3.2 Methanol solutions

Comparing the χ(k) data and χ(R) data in Figure 4d, we can find that they are very different from the water solution. The χ(k) data not only have different amplitudes but also different frequencies, which indicates the change of both coordination number and bond length. By comparing the χ(R) data, the spectral shape and bond length are also different. It suggests a new scattering path around the Ca^{2+} at a high concentration in methanol, which is different from water solutions. It is worth mentioning that the number of coordination O around Ca^{2+} in 0.5 mol/L $CaCl_2$ methanol solution and $CaCl_2 \cdot 6H_2O$ are the same by the analysis of XANES. The best fitting for 0.5mol/L Ca^{2+} in methanol shown in Figure 4e is about 7.1 methanol around Ca^{2+} with two distances. Near one is 3.7 oxygen atoms scatters with 2.28 Å and far one is 3.4 oxygen atoms scatters with 2.44 Å, rather than a single shell of nine oxygen atoms scatters. We can also verify this structure from DFT geometry optimization. As shown in Figure S9c, when 7 methanol molecules around the Ca^{2+}, the methanol molecules are divided into two distances. Moreover, some researchers found that there existing extensive Ca-Cl contact ion pairs in 2.0 mol/L[10, 16]. Referring to previous results and the differences in the χ(R) spectrum shape for different concentrations in methanol, we introduce a Ca-Cl pathway to fit the χ(R) spectrum for 3.0 mol/L $CaCl_2$ in methanol. Finally, we find that the best fitting for 3.0 mol/L $CaCl_2$ in methanol (Figure 4f) is consistent with the previous results. There are 2.5 methanol molecular at the 2.23 Å around

the Ca^{2+}, 3.3 methanol molecular with 2.39 Å at a little far away, and a Cl^- forming the contact ion pair around the Ca^{2+} at 2.83 Å. The detailed fitting parameters are also shown in Table S3.

3.4. DFT Calculations

We used DFT calculations to model the Ca^{2+} environments. We started with an initial guess of an Oh $Ca(H2O)_6^{2+}$ model which was built from scratch in Gaussview, with all the H_2O molecules evenly spaced. The optimized structure ended up with some obvious O-Ca-O angle distortions and open space for potentially more ligands. The number of H_2O molecules in the initial guess then kept increasing from 6 all the way to 10. We find that in the optimized structure of Ca^{2+} with 9 and 10 H_2O molecules, only ~ 8 water can remain in the first shell while the rest are repelled to the outer shell (>3.5 Å), which suggests the optimized coordination number for Ca^{2+} in diluted aqueous solution is 8. The detailed result is shown in Figure S8.

Then, similar procedures were done on Ca^{2+} with CH_3OH molecules surrounded. We also tried different numbers of the CH_3OH molecules as initial guesses. Similarly, in the optimized structure of Ca^{2+} with 10 CH_3OH molecules, only ~ 7 methanols can remain in the first shell. And the optimized structure of Ca^{2+} with 7 CH_3OH molecules is divided into two Ca-O distance, range from 2.3 to 2.5 Å, which is also consistent with EXAFS fitting results of 0.5 mol/L methanol solution. The detailed result is shown in Figure S9.

The simulated spectra by TD-DFT were used to help peak assignments in XANES, and were presented in previous sections already.

4. DISCUSSION

4.1 Concentration dependence

Badyal and Albright suggested that the local hydration environment of Ca^{2+} is independent of concentration, while Megyes *et al.* say the opposite. In this study, our experimental results support Megyes's argument and we show that the number of solvent molecules in the first solvation decreases with increasing Ca^{2+} concentration. From the XANES spectra of Ca^{2+} at

different concentrations in Figure 2, all peaks shift gradually with increasing Ca^{2+} concentration. Considering that water is a polar molecule with the more electronegative O pointing toward Ca^{2+}, more bonded water will donate more negative partial charge to the center Ca^{2+}. For that reason, the changes in the XANES spectrum indicate the change in the number of coordination water molecules. Similar trends were also found in the Ca K-edge XAENS spectrum of both methanol and ethanol solutions. Thus peaks shifts of the XANES provide direct evidence that the number of coordination solvent decreases with increasing Ca^{2+} concentration. The same conclusion can also be obtained by fitting the EXAFS region of the spectra at different concentrations (Figure 4).

4.2 Solvents dependence

In this study, we have measured Ca K-edge XAFS of $CaCl_2$ in different solvents. At the same concentration, the coordination number of Ca^{2+} of the nearest shell in aqueous solution is higher than in methanol solution, and it is higher in methanol solution than in ethanol solution, based on the XANES and EXAFS fittings. This is not surprising because bulkier ligands have more steric repulsion thus lead to a lower coordination number. What is more interesting is we need a Cl^- anion in the first solvation shell of Ca^{2+} to fit the EXAFS in methanol solutions at high concentration. This suggests water, as a more polar solvent, does a better job in solvating and separating the cations and anions. Methanol, which is less polar, has weak charge-dipole interactions, thus the cations and anions tend to have more direct interactions to minimize the total free energy of the system. This could also explain the relatively lower solubility of $CaCl_2$ in methanol (29.2 g per 100 g at 20 °C) than in water (74.5 g per 100 g at 20 °C).

4.3 First solvation shell fine structure

While neutron diffraction could give the long-range order structure for all interactions, the EXAFS has the advantage of obtaining an accurate structure in the local environment. In this study, we need to use two different Ca-O distances in the first shell to obtain a decent fit in methanol solution. This suggests not all the Ca-OH_4C in the first solvation shell have exactly the

same distances. Similar results can also be found in the DFT simulations if we turn the symmetry off. Notice what we were measuring are actually systems under dynamic equilibrium, with solvent ligands coming on and off each ion, thus some solvent ligands are in exchange with free ligands in the bulk, while others are tightly bonded to the ions. Fortunately, EXAFS is sensitive enough to catch the different bond distances of the tight bonds and loose bonds and could provide an average fine structure of the first solvation shell. We believe different techniques, especially at different temperatures, will give slightly different conclusions, and all the techniques need to be combined together to have a better understanding of the big picture of the system.

4.4 PCM effect in DFT calculations

In this study, it is important to consider the solvent effect in bulk outside the cluster we are modeling using DFT. One can choose to either add another layer of solvent molecules or to introduce the polarizable continuum model (PCM), which is a commonly used method in DFT. Here, we evaluate the effect of PCM vs explicitly modeling the outer shell solvation environment using real water molecules. The results for the first solvation shell only, and the second solvation shell included, in both vacuum and PCM are shown in Table 1 and Figure S10.

Table 1: Test of PCM effect

		The number of Nearest H_2O	First shell distance (Å)
First solvation shell only (10 H_2O molecules)	Vacuum	8	2.41-2.61
	PCM	8	2.42-2.50
Second solvation shell included (24 H_2O molecules)	Vacuum	8	2.43-2.60
	PCM	8	2.45-2.55

All methods give similar geometric structures according to Table 1. Because TD-DFT simulations only focus on the 1s to the valence transition on the Ca in the center, it is not surprising that the variations on the outer shell have little impact on the final results. Thus although explicitly including second shell water molecules can better model the H-bond network, they are computationally more expensive. Given that the PCM method can model the inner shell

with reasonable performance, we will stick with it for the rest of the study.

4.5 Extend the calculations on other metal ions

To further extend our study to a more general level, we used the experimental calibrated DFT parameters, to explore the solvation environment for some other metal ions in aqueous solutions, and the results are listed in Table 2. All the geometry optimizations were started with the same initial guess, with one metal ion in the center, and 10 water molecules around evenly spaced. Note here we did not consider other cations or anions in the system, thus the model only represents a diluted solution scenario.

Table 2 First shell environment for some cations in aqueous solution

Metal	Charge	Ionic radius (pm)	Coordination Number # by exp	M-H2O distance (Å) by exp	Coordination Number# by DFT	M-H2O distance (Å) by DFT
Na	1+	102	5[51]	2.4	4	2.39-2.46
K	1+	138	6[51-52]	2.9-3.4	5	2.29-2.40
Mg	2+	72	6[53]	2.12	6	2.06-2.10
Ca	2+	100	9[a]	2.39	8	2.42-2.50
Al	3+	57	6[54]	1.90	6	1.90-1.93

a: this article

Na^+ and Ca^{2+} have similar ionic size, but because Na^+ has less positive charge than Ca^{2+}, it has a lower coordination number. Mg^{2+} and Ca^{2+} have the same charge, but Mg^{2+} has a smaller size, thus more steric repulsion the ligand water molecules, which then leads to less coordination number. For the same reason, K^+ has more coordination numbers and longer M-H2O distance than Na^+. Al^{3+}, although it has a more positive charge, the ionic size is much more contracted, and the more pronouncing steric effect cancels the charge effect.

The DFT calculations with the parameters calibrated in this study did a decent job of predicting the solvation environment of other metal ions as well. It is going to be useful in

finding a general trend for the ion solvation effect. A more systematic study on that subject deserves more effort in the future, both theoretically and experimentally.

5. CONCLUSION

The XAFS results show a concentration dependence of the solvation structure around Ca^{2+} in different solvents. By comparing the XANES spectra of the $CaCl_2$ in water to those of reference compounds in solid-state forms, such as the crystalline hydrates, we derive the essential solvation structure picture of the fully hydrated Ca^{2+} ions, even when the concentrations of Ca^{2+} in water reaches the saturated concentration. Based on the results of XANES and EXAFS of $CaCl_2$ in water, we learn that the number of nearest coordination water decreases from about 9 to 3 with the concentration from 0.5 mol/L to saturation. The solvation structure of the first shell for 0.5 M is a single layer structure with 9 water around Ca^{2+}. But the solvation structure of the first shell for 10.0 M is divided into two distances, where only about 3 water molecules are in slightly shorter distance. In methanol, the solvation structure for 0.5mol/L Ca^{2+} in methanol also has two distance with 3.7 methanol at a slightly shorter distance, and 3.4 methanol at longer distance. Although there are also two different Ca-O distances at saturated concentration, we find the existence of the contact ion pair. The difference of the solvation structure between water and methanol at the same concentration are due to the difference in polarity and size of solvent molecules. This study is the first time to systematically compare the solvation structure in various polar molecules solvents and reveal the accuracy solvation structure of the first shell rather than only a coordination number. Meanwhile, the DFT calculations with the parameters calibrated in this study did a decent job of predicting the solvation environment of other metal ions as well to further extend our study to a more general level.

ASSOCIATED CONTENT

Supporting Information

Supporting Information is available free online.

Ca L-edge XAS spectra of three solid reference samples. TD-DFT calculated the transitions of three solid reference samples. Ca K-edge XANES of $CaCl_2 \cdot 6H_2O$_solid, $CaCl_2 \cdot 6H_2O$_liquid, and 10.0 M. Ca K-edge XAS for different concentration $CaCl_2$ in methanol and ethanol. energy shift and intensity evolution of peak D at the Ca K-edge with different concentrations in methanol and ethanol. pre-edge spectra of the Ca K-edge for solid and liquid samples. Peak A fitting of XANES. XANES spectra of Ca K-edge for 1.0mol/L, 1.5mol/L, 3.0mol/L $CaCl_2$ in water, methanol, and ethanol. The Fourier transform spectrum of the EXAFS for 10.0 M and $CaCl_2 \cdot 6H_2O$_liquid. The Fourier transform spectrum of the EXAFS and fit for 10.0mol/L $CaCl_2$. geometry optimization of H_2O and methanol around Ca^{2+}.

AUTHOR INFORMATION

Corresponding Author:

Xiaosong Liu Email: xliu3@mail.sim.ac.cn Telephone number:+86-021-62511070-3303
Jinghua Guo Email: JGuo@lbl.gov Telephone number: +1-510-495-2230

Notes:

The authors declare no competing financial interest.

ACKNOWLEDGMENTS

This research used resources of the Advanced Light Source, which is a DOE Office of Science User Facility under contract no. DE-AC02-05CH11231. We thank Sirine Fakra for support on BL10.3.2. of Advanced Light Source. This research is supported by the National Natural Science Foundation of China (No. 11227902, U1632269) and the National Key Research and Development Program of China (2019YFA0405601). This research is also supported by the UCAS Joint Ph.D. training program.

REFERENCES

1. Aziz, E. F.; Freiwald, M.; Eisebitt, S.; Eberhardt, W., Steric hindrance of ion-ion interaction in electrolytes. *Physical Review B* **2006,** *73* (7).
2. Li, Z.; Mu, X.; Zhao-Karger, Z.; Diemant, T.; Behm, R. J.; Kubel, C.; Fichtner, M., Fast kinetics of multivalent intercalation chemistry enabled by solvated magnesium-ions into self-established metallic layered materials. *Nat Commun* **2018,** *9* (1), 5115.
3. Frank, P.; Benfatto, M.; Qayyam, M.; Hedman, B.; Hodgson, K. O., A high-resolution XAS study of aqueous Cu(II) in liquid and frozen solutions: pyramidal, polymorphic, and non-centrosymmetric. *J Chem Phys* **2015,** *142* (8), 084310.
4. Migliorati, V.; Zitolo, A.; Chillemi, G.; D'Angelo, P., Influence of the Second Coordination Shell on the XANES Spectra of the Zn2+ Ion in Water and Methanol. *ChemPlusChem* **2012,** *77* (3), 234-239.
5. Wang, K.; Xu, F.; Cao, S.; Wang, H.; Wei, Y.; Shao, X.; Zhou, W.; Zheng, Y., Effects of exogenous calcium chloride (CaCl2) and ascorbic acid (AsA) on the γ-aminobutyric acid (GABA) metabolism in shredded carrots. *Postharvest Biology and Technology* **2019,** *152*, 111-117.
6. Granados, M. L.; Poves, M. D. Z.; Alonso, D. M.; Mariscal, R.; Galisteo, F. C.; Moreno-Tost, R.; Santamaría, J.; Fierro, J. L. G., Biodiesel from sunflower oil by using activated calcium oxide. *Applied Catalysis B: Environmental* **2007,** *73* (3-4), 317-326.
7. Monti, D.; Ponrouch, A.; Araujo, R. B.; Barde, F.; Johansson, P.; Palacin, M. R., Multivalent Batteries-Prospects for High Energy Density: Ca Batteries. *Front Chem* **2019,** *7*, 79.
8. N. A. Hewish, G. W. N. J. E. E., Environment of Ca2+ ions in aqueous solvent. *Nature* **1982**.
9. Simonson, A. A. C. a. J. M., The structure of CaCl2 aqueous solutions over a wide range of concentration. Interpretation of diffraction experiments via molecular simulation. *J Chem Phys* **2003,** *119*, 8052.
10. Megyes, T.; Grósz, T.; Radnai, T.; Bakó, I.; Pálinkás, G., Solvation of Calcium Ion in Polar Solvents: An X-ray Diffraction and ab Initio Study. *The Journal of Physical Chemistry A* **2004,** *108* (35), 7261-7271.
11. Badyal, Y. S.; Barnes, A. C.; Cuello, G. J.; Simonson, J. M., Understanding the Effects of Concentration on the Solvation Structure of Ca2+in Aqueous Solution. II: Insights into Longer Range Order from Neutron Diffraction Isotope Substitution. *The Journal of Physical Chemistry A* **2004,** *108* (52), 11819-11827.
12. Fulton, J. L.; Heald, S. M.; Badyal, Y. S.; Simonson, J. M., Understanding the Effects of Concentration on the Solvation Structure of Ca2+in Aqueous Solution. I: The Perspective on Local Structure from EXAFS and XANES. *The Journal of Physical Chemistry A* **2003,** *107* (23), 4688-4696.
13. Albright, J. N., X-Ray Diffraction Studies of Aqueous Alkaline-Earth Chloride Solutions.

The Journal of Chemical Physics **1972,** *56* (8), 3783-3786.
14. Dang, L. X.; Schenter, G. K.; Fulton, J. L., EXAFS Spectra of the Dilute Solutions of Ca2+and Sr2+in Water and Methanol. *The Journal of Physical Chemistry B* **2003,** *107* (50), 14119-14123.
15. Kosztolányi, T.; Bakó, I.; Pálinkás, G., Molecular dynamics study of CaCl2 in liquid methanol. *Journal of Molecular Liquids* **2006,** *126* (1-3), 1-8.
16. Megyes, T.; Bálint, S.; Bakó, I.; Grósz, T.; Radnai, T.; Pálinkás, G., Solvation of calcium ion in methanol: Comparison of diffraction studies and molecular dynamics simulation. *Chemical Physics* **2006,** *327* (2-3), 415-426.
17. Martinek, T.; Duboue-Dijon, E.; Timr, S.; Mason, P. E.; Baxova, K.; Fischer, H. E.; Schmidt, B.; Pluharova, E.; Jungwirth, P., Calcium ions in aqueous solutions: Accurate force field description aided by ab initio molecular dynamics and neutron scattering. *J Chem Phys* **2018,** *148* (22), 222813.
18. Rudolph, W. W.; Irmer, G., Hydration of the calcium(II) ion in an aqueous solution of common anions (ClO4-, Cl-, Br-, and NO3-). *Dalton Trans* **2013,** *42* (11), 3919-35.
19. Kohagen, M.; Mason, P. E.; Jungwirth, P., Accurate description of calcium solvation in concentrated aqueous solutions. *J Phys Chem B* **2014,** *118* (28), 7902-9.
20. Tucceri, R., A review about the surface resistance technique in electrochemistry. *Surface Science Reports* **2004,** *56* (3-4), 85-157.
21. Ohtaki, H.; Radnai, T., Structure and dynamics of hydrated ions. *Chemical Reviews* **1993,** *93* (3), 1157-1204.
22. Naftel, S. J.; Sham, T. K.; Yiu, Y. M.; Yates, B. W., CalciumL-edge XANES study of some calcium compounds. *Journal of Synchrotron Radiation* **2001,** *8* (2), 255-257.
23. Metzler, R. A.; Rez, P., Polarization dependence of aragonite calcium L-edge XANES spectrum indicates c and b axes orientation. *J Phys Chem B* **2014,** *118* (24), 6758-66.
24. Politi, Y.; Metzler, R. A.; Abrecht, M.; Gilbert, B.; Wilt, F. H.; Sagi, I.; Addadi, L.; Weiner, S.; Gilbert, P. U., Transformation mechanism of amorphous calcium carbonate into calcite in the sea urchin larval spicule. *Proc Natl Acad Sci U S A* **2008,** *105* (45), 17362-6.
25. Gong, Y. U.; Killian, C. E.; Olson, I. C.; Appathurai, N. P.; Amasino, A. L.; Martin, M. C.; Holt, L. J.; Wilt, F. H.; Gilbert, P. U., Phase transitions in biogenic amorphous calcium carbonate. *Proc Natl Acad Sci U S A* **2012,** *109* (16), 6088-93.
26. Jalilehvand, F.; Spångberg, D.; Lindqvist-Reis, P.; Hermansson, K.; Persson, I.; Sandström, M., Hydration of the Calcium Ion. An EXAFS, Large-Angle X-ray Scattering, and Molecular Dynamics Simulation Study. *Journal of the American Chemical Society* **2001,** *123* (3), 431-441.
27. Spångberg, D.; Hermansson, K.; Lindqvist-Reis, P.; Jalilehvand, F.; Sandström, M.; Persson, I., Model Extended X-ray Absorption Fine Structure (EXAFS) Spectra from Molecular Dynamics Data for Ca2+and Al3+Aqueous Solutions. *The Journal of Physical Chemistry B* **2000,** *104* (45), 10467-10472.
28. Antalek, M.; Pace, E.; Hedman, B.; Hodgson, K. O.; Chillemi, G.; Benfatto, M.; Sarangi, R.; Frank, P., Solvation structure of the halides from x-ray absorption spectroscopy. *J Chem Phys*

2016, *145* (4), 044318.
29. Migliorati, V.; D'Angelo, P., A quantum mechanics, molecular dynamics and EXAFS investigation into the Hg2+ ion solvation properties in methanol solution. *RSC Advances* **2013,** *3* (43).
30. Engstrom, L. M.; Brinkmeyer, M. K.; Ha, Y.; Raetz, A. G.; Hedman, B.; Hodgson, K. O.; Solomon, E. I.; David, S. S., A zinc linchpin motif in the MUTYH glycosylase interdomain connector is required for efficient repair of DNA damage. *J Am Chem Soc* **2014,** *136* (22), 7829-32.
31. Mason, J. L.; Harb, H.; Huizenga, C. D.; Ewigleben, J. C.; Topolski, J. E.; Hratchian, H. P.; Jarrold, C. C., Electronic and Molecular Structures of the CeB6 Monomer. *J Phys Chem A* **2019,** *123* (10), 2040-2048.
32. Thompson, L. M.; Jarrold, C. C.; Hratchian, H. P., Explaining the MoVO4(-) photoelectron spectrum: Rationalization of geometric and electronic structure. *J Chem Phys* **2017,** *146* (10), 104301.
33. Ha, Y.; Arnold, A. R.; Nunez, N. N.; Bartels, P. L.; Zhou, A.; David, S. S.; Barton, J. K.; Hedman, B.; Hodgson, K. O.; Solomon, E. I., Sulfur K-Edge XAS Studies of the Effect of DNA Binding on the [Fe4S4] Site in EndoIII and MutY. *J Am Chem Soc* **2017,** *139* (33), 11434-11442.
34. Ha, Y.; Tenderholt, A. L.; Holm, R. H.; Hedman, B.; Hodgson, K. O.; Solomon, E. I., Sulfur K-edge X-ray absorption spectroscopy and density functional theory calculations on monooxo Mo(IV) and bisoxo Mo(VI) bis-dithiolenes: insights into the mechanism of oxo transfer in sulfite oxidase and its relation to the mechanism of DMSO reductase. *J Am Chem Soc* **2014,** *136* (25), 9094-105.
35. Ravel, B.; Newville, M., ATHENA, ARTEMIS, HEPHAESTUS: data analysis for X-ray absorption spectroscopy using IFEFFIT. *Journal of Synchrotron Radiation* **2005,** *12* (4), 537-541.
36. Frisch, M. J., Trucks, G. W., Schlegel, H. B., Scuseria, G. E., Robb, M. A., Cheeseman, J. R., Scalmani, G., Barone, V., Mennucci, B., Petersson, G. A., Nakatsuji, H., Caricato, M., Li, X., Hratchian, H. P., Izmaylov, A. F., Bloino, J., Zheng, G., Sonnenberg, J. L., Hada, M., Ehara, M., Toyota, K., Fukuda, R., Hasegawa, J., Ishida, M., Nakajima, T., Honda, Y., Kitao, O., Nakai, H., Vre., Brothers, E., Kudin, K. N., Staroverov, V. N., Kobayashi, R., Normand, J., Raghavachari, K., Rendell, A., Burant, J. C., Iyengar, S. S., Tomasi, J., Cossi, M., Rega, N., Millam, J. M., Klene, M., Knox, J. E., Cross, J. B., Bakken, V., Adamo, C., Jaramillo, J., Gomperts, R., Stratmann, R. E., Yazyev, O., Austin, A. J., Cammi, R., Pomelli, C., Ochterski, J. W., Martin, R. L., Morokuma, K., Zakrzewski, V. G., Voth, G. A., Salvador, P., Dannenberg, J. J., Dapprich, S., Daniels, A. D., Farkas, Foresman, J. B., Ortiz, J. V., Cioslowski, J., and Fox, D. J *Gaussian 09*, B.01; Wallingford CT, 2009.
37. Neese, F., The ORCA program system. *Wiley Interdisciplinary Reviews: Computational Molecular Science* **2012,** *2* (1), 73-78.
38. McQuilken, A. C.; Ha, Y.; Sutherlin, K. D.; Siegler, M. A.; Hodgson, K. O.; Hedman, B.; Solomon, E. I.; Jameson, G. N.; Goldberg, D. P., Preparation of non-heme {FeNO}7 models of

cysteine dioxygenase: sulfur versus nitrogen ligation and photorelease of nitric oxide. *J Am Chem Soc* **2013,** *135* (38), 14024-7.
39. Grimme, S.; Ehrlich, S.; Goerigk, L., Effect of the damping function in dispersion corrected density functional theory. *J Comput Chem* **2011,** *32* (7), 1456-65.
40. Grimme, S.; Antony, J.; Ehrlich, S.; Krieg, H., A consistent and accurate ab initio parametrization of density functional dispersion correction (DFT-D) for the 94 elements H-Pu. *J Chem Phys* **2010,** *132* (15), 154104.
41. Ekstrom, U.; Visscher, L.; Bast, R.; Thorvaldsen, A. J.; Ruud, K., Arbitrary-Order Density Functional Response Theory from Automatic Differentiation. *J Chem Theory Comput* **2010,** *6* (7), 1971-80.
42. Weigend, F.; Ahlrichs, R., Balanced basis sets of split valence, triple zeta valence and quadruple zeta valence quality for H to Rn: Design and assessment of accuracy. *Phys Chem Chem Phys* **2005,** *7* (18), 3297-305.
43. Bever A, K. v.; Nieuwenkamp, W., Die Kristallstruktur von Calciumchlorid, CaCl2. In *Zeitschrift für Kristallographie - Crystalline Materials*, 1935; Vol. 90, p 374.
44. Leclaire, A.; Borel, M. M., Le dichlorure de calcium dihydrate. *Acta Crystallographica Section B* **1977,** *33* (5), 1608-1610.
45. Leclaire, A.; Borel, M. M., Le dichlorure et le dibromure de calcium hexahydrates. *Acta Crystallographica Section B* **1977,** *33* (9), 2938-2940.
46. Cicconi, M. R.; de Ligny, D.; Gallo, T. M.; Neuville, D. R., Ca neighbors from XANES spectroscopy: A tool to investigate structure, redox, and nucleation processes in silicate glasses, melts, and crystals. *American Mineralogist* **2016,** *101* (5), 1232-1235.
47. Martin-Diaconescu, V.; Gennari, M.; Gerey, B.; Tsui, E.; Kanady, J.; Tran, R.; Pecaut, J.; Maganas, D.; Krewald, V.; Goure, E.; Duboc, C.; Yano, J.; Agapie, T.; Collomb, M. N.; DeBeer, S., Ca K-edge XAS as a probe of calcium centers in complex systems. *Inorg Chem* **2015,** *54* (4), 1283-92.
48. Sugiura, C., K-x-ray spectra and electronic band structures of MgCl2, CaCl2, SrCl2, and BaCl2. *Physical Review B* **1974,** *9* (6), 2679-2683.
49. Siritapetawee, J.; Limphirat, W.; Kantachot, C.; Kongmark, C., The effects of metal ions in Euphorbia cf. lactea latex on the fibrinogenolytic activity of a plant protease. *Appl Biochem Biotechnol* **2015,** *175* (1), 232-42.
50. Sowrey, F. E.; Skipper, L. J.; Pickup, D. M.; Drake, K. O.; Lin, Z.; Smith, M. E.; Newport, R. J., Systematic empirical analysis of calcium–oxygen coordination environment by calcium K-edge XANES. *Phys. Chem. Chem. Phys.* **2004,** *6* (1), 188-192.
51. Ansell, S.; Barnes, A. C.; Mason, P. E.; Neilson, G. W.; Ramos, S., X-ray and neutron scattering studies of the hydration structure of alkali ions in concentrated aqueous solutions. *Biophys Chem* **2006,** *124* (3), 171-9.
52. Soper, A. K.; Weckstrom, K., Ion solvation and water structure in potassium halide aqueous solutions. *Biophys Chem* **2006,** *124* (3), 180-91.
53. Pálinkás, G.; Radnai, T., Hydration Shell Structures in an MgCl2 Solution from X-Ray and MD Studies. *Zeitschrift für Naturforschung A* **1982,** *37* (9).

54. Caminiti, R.; Licheri, G.; Piccaluga, G.; Pinna, G.; Radnai, T., Order phenomena in aqueous AlCl3 solutions. *The Journal of Chemical Physics* **1979,** *71* (6), 2473-2476.

For Table of Contents Only